CrossMark

A Spectral Element Method to Compute Earth's Free Core Nutation

Mian Zhang[1,2] and Cheng-Li Huang[1,2]
[1] CAS Key Laboratory of Planetary Sciences, Shanghai Astronomical Observatory, Chinese Academy of Sciences, Shanghai 200030, China; mzhang@shao.ac.cn
[2] School of Astronomy and Space Sciences, University of Chinese Academy of Sciences, Beijing 100049, China

Abstract

The Free Core Nutation (FCN) is a rotational mode caused by non-alignment of the rotation axis of the core and of the mantle. Its period observed by VLBI and superconducting gravimetry is around 430 sidereal days (Sd) with precision of better than 1 Sd, while its "theoretical" period calculated by traditional approaches and a given Earth model ranges from 450 to 470 Sd. Their gap of about 30 Sd is significant compared with its observation precision. We propose a spectral element method to compute the period of FCN and obtain a period of 434 Sd which is very close to the observed value.

Key words: Earth – planets and satellites: interiors – methods: numerical

1. Introduction

The free motions, in the absence of the external torques produced by the gravitational forces exerted on the Earth by the Moon and Sun, conserve the Earth's total angular momentum. For a three-layer Earth without ocean that rotates and has nonzero ellipticity, there are four rotational modes: the Chandler wobble (CW) with predicted period from 306 to 435 sidereal days (Sd) due to the combined effects of the mantle elasticity and the presence of the outer core and oceans; the Free Core Nutation (FCN) with a period of about 430 Sd in the celestial frame (Zhou et al. 2016; Malkin 2017; Cui et al. 2018); the free inner-core nutation with a supposed long period about 1000 Sd (Mathews et al. 2002) in the celestial frame; and the inner-core wobble with a longer period in the terrestrial frame. The frequency of the FCN resonates with the forced annual nutation that plays an important role in the nutational responses of the Earth.

FCN is a normal or eigenmode of the rotating Earth, if only there is a fluid core which is elliptical rather than spherical, and it is related to slight misalignment of the rotation axes of the Earth's fluid core and mantle. By solving the dynamic Equations (3) and (6) (with a set of boundary conditions) describing the motion of the mantle and the fluid core in which the self-gravitation (including the gravitational coupling between the mantle and the core) and Coriolis force play important roles in the dynamics, one can obtain a series of eigen solutions, and FCN should be one of these eigenmodes. If following traditional representation of the displacement vector field $\overrightarrow{u}$ by a coupled chain of spheroidal and toroidal components, among of which the toroidal component of spherical harmonics degree 1 and order 1, $\overrightarrow{T}_1^1$, represents a rigid rotation around an axis in the equatorial plane, one can see

that, additional to this rigid rotation component $\overrightarrow{T}_1^1$, there are also many other components in the displacement/velocity field, and that FCN is only one (of $\overrightarrow{T}_1^1$) of the many solutions of the whole dynamical system.

From processing the observed VLBI data of Earth's rotation and superconducting gravimeter data of Earth's tides, its period is about 430 Sd with precision better than 1 Sd (Zhou et al. 2016; Malkin 2017; Cui et al. 2018) seen from a celestial reference frame and is a retrograde mode; this mode is also known as the Nearly Diurnal Free Wobble (NDFW) because it has a period close to one day seen from a terrestrial reference frame (Seyed-Mahmoud & Rogister 2021). Its period depends on (therefore reflects on) the physics and dynamics of the core and the mantle, especially near the core–mantle boundary (CMB). Hence, FCN connects Earth's deep interior and the celestial observation of Earth's rotation and it is a very important "telescope" for the study of the Earth's deep interior. However, the "theoretical" FCN period calculated by traditional approaches and a given Earth model ranges from 450 to 470 Sd. Their gap of about 30 Sd is significant compared with its observation precision.

There are four approaches for theoretical computation of FCN period. The first is based on the conservation of the angular momentum which was originally proposed by Hough (1895), who used an Earth model composed of a homogeneous rigid shell and an incompressible homogeneous fluid core. This model is transformed into an oblate by Earth's rotation, and is called Hough–Poincaré model. From angular momentum conservation law, FCN frequency can be written as (Rochester et al. 1974)

$$\sigma = -\Omega\left(1 + \frac{Ae_1}{A_0}\right), \tag{1}$$

where e_1 is the flattening of CMB, Ω is the rotation speed of Earth, A and A_0 are the equatorial moments of inertia of the Earth and the mantle respectively. Hough computed the period of NDFW in a rotating frame. He pointed out that there would be a nutation associated with this mode with frequency

$$\lambda = -\Omega \frac{A e_1}{A_0}. \qquad (2)$$

This mode became known as FCN in the 1980s (Seyed-Mahmoud & Rogister 2021).

This approach has the virtue of simplicity, but its FCN result deviates much from the real one due to the simple model. The 350 days period (Rochester et al. 1974) is for an Earth model with rigid mantle. That is the same as Poincare and Hough's results. Mathews et al. (1991) also used the angular momentum approach and found a period of 468 Sd for an Earth model with elastic mantle and inner core.

The second approach is based on the Runge–Kutta integration on the linear momentum description of the dynamical equations. Smith (1974) applied this method to solve for the Earth's normal modes including FCN. He extended and applied the Generalized Spherical Harmonics based on previous studies, e.g., Phinney & Burridge (1973) (see Huang & Liao 2003 for corrections and comment), to transform vectors and tensors in the governing equations for the small periodic oscillations of an oblate spheroidal rotating elastic isotropic Earth model from an ellipsoidal domain to an equivalent spherical domain (ESD). Application of this approach yields periods for FCN ranging from 450 Sd to 460 Sd (Wahr 1981; Dehant 1990; Huang et al. 2001; Rogister 2001) for the Preliminary Reference Earth Model (Dziewonski & Anderson 1981). There is still a gap between these results and the observed period of FCN.

The third approach is based on the variational principle (Johnson & Smylie 1977; Moon 1982; Smylie et al. 1992). This variational principle is numerically implemented by a finite element approach. Jiang & Smylie (1996) computed FCN mode based upon a variational principle of the dynamics of the liquid outer core and found a period of 450 Sd.

There are many publications trying to interpret this large gap of the FCN period by various assumptions. Gwinn et al. (1986), and Dehant & Defraigne (1997) explained this discrepancy by non-hydrostatic ellipticity of the CMB. Huang et al. (2001) showed that the calculated FCN period would agree with the observed by modifying ϵ_{CMB} from 0.002547 to 0.002666 (a 4.7% increase). The excess over the hydrostatic equilibrium value for ϵ_{CMB} estimated by Mathews et al. (2002) was between 3.7% and 3.9%. Buffett et al. (2002) tried to interpret this gap by the geomagnetic torque on the CMB, But Huang et al. (2011) showed that the assumed contribution of the coupling between geomagnetic field and nutation is about one order of magnitude smaller than the required to fill the gap (i.e., about 30 Sd), even using the same values of related parameters

(e.g., the electric conductivity, the thickness of the skin layer near the CMB, etc.) as adopted in Buffett et al. (2002).

However, these explanations are not proved: the real ellipticity of CMB and the geomagnetic torque on CMB are not known. There are also other possible explanations. The first is the inner core's differential rotation which proved by the seismic data (Song & Richards 1996; Song 2011). The second is the topography of the coremantle boundary. As the ellipticity of the CMB is a kind of topography, How do other kinds of topography (e.g., Y_2^1, Y_3^2, Y_4^0) affect FCN? However, the above three approaches cannot test these two hypotheses. So we developed the fourth approach.

The fourth approach is based on the Galerkin method. This Galerkin method was first used in studying the inertial modes of a compressible and stratified fluid core with rigid boundaries (Seyed-Mahmoud 1994; Seyed-Mahmoud et al. 2007, 2015) with the 3-Potential description, the free wobble/nutation modes of a simple Earth model with a rotating, inviscid, homogeneous and incompressible fluid core contained in a spherical shell with rigid boundaries (Seyed-Mahmoud et al. 2017). Zhang & Huang (2014) tried first to apply the stratified Galerkin method which is also called as the spectral element method (Karniadakis & Sherwin 2013), to study FCN period for a more real Earth model (PREM), and their calculated FCN period is 435 Sd, neither increasing the CMB ellipticity from its hydrostatic values as mentioned above, nor assuming of the geomagnetic contribution. Zhang & Huang (2019) used this approach to study the effect of the Earth's differential rotation of the inner core on the period of the FCN, and proved that the inner core's differential rotation cannot interpret this gap. But Zhang & Huang (2019) simply gave a very briefly introduction of this method, and did not give details. Kamruzzaman (2021) applied the Galerkin method to solve the dynamical equations with boundary conditions to include the first order ellipticity using the Clairaut coordinate system and the spherical harmonics, and found a period of 432 Sd. In this paper, we give details of this method, and extend truncation from $\overrightarrow{T}_1^1 + (\overrightarrow{R}_2^1 + \overrightarrow{S}_2^1) + \overrightarrow{T}_3^1$ to $\overrightarrow{T}_1^1 + (\overrightarrow{R}_2^1 + \overrightarrow{S}_2^1) + \overrightarrow{T}_3^1 + (\overrightarrow{R}_4^1 + \overrightarrow{S}_4^1) + \overrightarrow{T}_5^1$.

2. Dynamical Equations and Boundary Conditions

In solid mantle and inner core, we take

$$\rho_0 \omega^2 \overrightarrow{u} - 2i\rho_0 \omega \overrightarrow{\Omega} \times \overrightarrow{u} + \rho_0 \nabla V_1 + \rho_0 \nabla(\overrightarrow{u} \cdot \overrightarrow{g_0})$$
$$- \rho_0 \overrightarrow{g_0}(\nabla \cdot \overrightarrow{u}) + \nabla \cdot \overleftrightarrow{S} = 0 \qquad (3)$$

as the equation governing the small periodic oscillations of a rotating self-gravitational elastic isotropic Earth model, disturbed from hydrostatic equilibrium (Dahlen 1972). In Equation (3), ρ_0, V_1 and $\overrightarrow{g_0}$ are density, incremental gravitational potential, and the initial gravity in an equilibrium configuration respectively; 86164.1 s is the length of a sidereal

day, which is the Earth's rotation period. $\overrightarrow{\Omega}$ is the Earth's angular velocity, its value is

$$|\mathbf{\Omega}| = 2\pi/\text{sidereal day} = 2\pi/86164.1 \text{ s}$$
$$\approx 7.292115 \times 10^{-5} \text{ s}^{-1}. \tag{4}$$

And the mass element dm in an equilibrium configuration experiences a small displacement $\overrightarrow{u}$ with an oscillation's angular frequency ω. In Equation (3), $\overleftrightarrow{S}$ is the Lagrangian variation of the Cauchy stress tensor due to the deformation and is given by the following equation for elastic isotropic body

$$\overleftrightarrow{S} = \lambda(\nabla \cdot \boldsymbol{u})\overleftrightarrow{I} + \mu[\nabla\boldsymbol{u} + (\nabla\boldsymbol{u})^T], \tag{5}$$

where λ, μ are Lamé parameters.

In fluid core,

$$\rho_0\omega^2\overrightarrow{u} - 2i\rho_0\omega\overrightarrow{\Omega} \times \overrightarrow{u} - \nabla p_1 + \rho_0\nabla V_1 + \rho_1\overrightarrow{g_0} = 0 \tag{6}$$

is the equation governing the isentropic small oscillations of a liquid core by the conservation laws for mass, momentum, gravitational flux and entropy (Rochester et al. 1989); see also Huang et al. (2004) for detail derivation and numerical integration method for the governing dynamical equation in fluid core.

Incremental density ρ_1 and pressure p_1 are defined as

$$\rho_1 = -\nabla \cdot (\rho_0\boldsymbol{u}), \tag{7}$$

and

$$p_1 = -\boldsymbol{u} \cdot \nabla p_0 + \alpha^2\rho_1 + \alpha^2\boldsymbol{u} \cdot \nabla\rho_0, \tag{8}$$

where p_0 is the pressure in an equilibrium configuration, and α is compressional wave speed. In the liquid core, the stress tensor takes the form

$$\overleftrightarrow{S} = -(p_1 + \boldsymbol{u} \cdot \nabla p_0)\overleftrightarrow{I}. \tag{9}$$

The incremental gravitational potential V_1 also satisfies the same format of Poisson's equation for the total potential V or the initial potential V_0 in hydrostatic equilibrium, i.e.,

$$\nabla^2 V_1 = 4\pi G\nabla \cdot (\rho_0\boldsymbol{u}), \tag{10}$$

in both fluid and solid layers.

Boundary conditions at the solid-liquid interfaces require continuity in

$$\{\hat{n} \cdot \overrightarrow{u}\}_-^+ = 0 \tag{11}$$

$$\{\hat{n} \cdot \overleftrightarrow{S}\}_-^+ = 0 \tag{12}$$

$$\{V_1\}_-^+ = 0 \tag{13}$$

$$\{\hat{n} \cdot [\nabla V_1 - 4\pi G\rho_0\overrightarrow{u}]\}_-^+ = 0. \tag{14}$$

Similarly, at the welded boundaries, i.e., solid–solid interfaces, boundary conditions require continuity in

$$\{\overrightarrow{u}\}_-^+ = 0 \tag{15}$$

$$\{\hat{n} \cdot \overleftrightarrow{S}\}_-^+ = 0 \tag{16}$$

$$\{V_1\}_-^+ = 0 \tag{17}$$

$$\{\hat{n} \cdot [\nabla V_1 - 4\pi G\rho_0\overrightarrow{u}]\}_-^+ = 0. \tag{18}$$

The boundary conditions on the Earth's free surface require

$$\{\hat{n} \cdot [\nabla V_1 - 4\pi G\rho_0\overrightarrow{u}]\}_-^+ = 0 \tag{19}$$

$$\{\hat{n} \cdot \overleftrightarrow{S}\}_-^+ = 0 \tag{20}$$

$$\{V_1\}_-^+ = 0, \tag{21}$$

where the corresponding parameters at the outer side (ρ_0^+, $\overleftrightarrow{S}^+$, etc.) can be adjusted according to various situations and assumptions.

3. Multiple Subdomains Spectral Method

In this work we show that the spectral method is an effective technique to solve the above equations. Suppose that an unknown function $u(x)$ satisfies a differential equation:

$$L[u(x)] = D, \tag{22}$$

where L is a linear differential operator. Spectral method represents $u(x)$ as a truncated series:

$$u(x) \approx u_N(x) = \sum_{n=0}^{N} c_n\eta_n(x), \tag{23}$$

where $\eta_n(x)$ are basis functions and c_n are their coefficients. This series is then put into differential Equation (22):

$$L\left[\sum_{n=0}^{N} c_n\eta_n(x)\right] = D. \tag{24}$$

By the Galerkin method, which can be regarded as one kind of the spectral methods, the above equation turns into a group of equations:

$$\int \iota_j(x)L\left[\sum_{n=0}^{N} c_n\eta_n(x)\right]dx = \int \iota_j(x)D \, dx, \tag{25}$$

where $\iota_j(x)$ are trial functions. By solving Equation (25) as well as the boundary conditions, we can obtain an approximate solution of the unknown function $u(x)$, which is $u_N(x)$.

For a complex Earth model, only one global domain is not enough to represent some characteristics, such as the densities and the toroidal displacement fields in fluid core and solid mantle. Instead, the whole global domain is partitioned into K disjoint subdomains. In the kth subdomain, an unknown function $u^{(k)}(x)$ is expressed as

$$u^{(k)}(x) \approx \sum_{n=0}^{N} c_n^{(k)}\eta_n^{(k)}(x), \tag{26}$$

where $\eta_n^{(k)}(x)$ are basis functions of kth subdomain and $c_n^{(k)}$ are their coefficients. So Equation (25) turns into K groups of

equations:

$$\int_{V^{(k)}} \iota_j^{(k)}(x) L^{(k)} \left[\sum_{n=0}^{N} c_n^{(k)} \eta_n^{(k)}(x) \right] dx$$
$$= \int_{V^{(k)}} D^{(k)} \, dx, \tag{27}$$

where $\iota_j^{(k)}(x)$ are trial functions in the kth subdomain and $L^{(k)}$ are their linear operators. Equation (27) will create a $K(N+1) \times K(N+1)$ matrix. Suppose that there are M boundary conditions:

$$B_i \left[\sum_{k=1}^{K} u^{(k)}(x) \right] = E_i, \quad i = 1, \cdots, M. \tag{28}$$

We use the Tau method (Karniadakis & Sherwin 2013) to combine these boundary conditions with Equation (27). The Tau method replaces M equations in Equation (27) with M boundary conditions in Equation (28). For instance, there are $N+1$ equations, then the Tau method usually replaces the last M equations with M boundary conditions. The unknown functions $u^{(k)}(x)$ in all K subdomains can be obtained by solving the new $K(N+1) \times K(N+1)$ matrix. The global $u(x)$ is the union of $u^{(k)}(x)$: $\bigcup_{k=1}^{K} u^{(k)}(x)$, which is like a sheaf in category theory. This spectral method on multiple subdomains is a kind of spectral element method (Boyd 2001; Karniadakis & Sherwin 2013), and we name it as the stratified Galerkin method here, as Galerkin's method is chosen to convert the continuous operator problem to the discrete problem.

4. Integration in Volumes

To solve the governing equations, these equations are usually transformed (Smith 1974) into a group of partial differential equations (PDEs), and the vectors of variables are integrated from Earth's center to surface with some certain initial values by Runge–Kutta method. Compared to this direct numerical integration of these variables, our approach is to directly integrate these governing equations containing variables that have no given value, which are manipulated as symbols.

Although the hydrostatic equilibrium figure is an ellipsoid, we still solve these equations in spherical coordinates, which makes symbolic operations of vector spherical harmonics and tensors more complex and tedious. We adopt a linear operator method similar to Rogister & Rochester (2004)'s. However, Kopal (1980) recommended a non-orthogonal coordinate system named "Clairaut" coordinates for the astrophysical research. The coordinate surfaces of this non-orthogonal coordinate system consist with the equilibrium surfaces of an equipotential ellipsoid. Wu (1993) and Seyed-Mahmoud & Moradi (2014) used Clairaut coordinates to study the dynamics of the fluid core. Rogister & Rochester (2004), Rochester et al. (2014), and Crossley & Rochester (2014) applied Clairaut coordinates to the linear momentum approach accurate to

second order in the ellipticity. Smith (1974) proposed a concept of ESD to deal with integration in the first-order approximated ellipsoid. ESD transforms an ellipsoid into a sphere, then parameters are modified with ellipticity. As a result, the final PDEs do not have θ or ϕ explicitly, and the vectors of variables are integrated only along the radius r's direction. However, ESD approach is difficult to deal with asymmetric models, for instance, it is difficult and complex to transform a surface with a Y_3^0 component or a Y_2^2 component to a spherical surface. Therefore, we do not follow the ESD, instead, we integrate the governing equations in shells of any figure (i.e., without assumption of any symmetricity) directly. Suppose that an asymmetric shell has an inner boundary:

$$r = R_{\text{in}} + \sum_{n,m} \xi_n^m Y_n^m(\theta, \phi), \tag{29}$$

and an outer boundary:

$$r = R_{\text{out}} + \sum_{n,m} \Xi_n^m Y_n^m(\theta, \phi), \tag{30}$$

where R_{in}, R_{out}, ξ_n^m, Ξ_n^m are all constants, and $Y_n^m(\theta, \phi)$ are spherical harmonics. If $\xi_n^m = 0$ and $\Xi_n^m = 0$, then this shell is a spheric shell; if only ξ_2^0 and Ξ_2^0 are not equal to 0, then this shell is a first-order ellipsoidal shell.

The volume between the inner and the outer boundaries is

$$\iiint dV = \int_{\theta=0}^{\pi} \int_{\phi=0}^{2\pi} \int_{R_{\text{in}}+\sum_n^m \xi_n^m Y_n^m(\theta,\phi)}^{R_{\text{out}}+\sum_n^m \Xi_n^m Y_n^m(\theta,\phi)} r^2 \sin\theta dr d\phi d\theta. \tag{31}$$

The integral of a vector equation $L\chi$ in this volume with a trial function vector $\overrightarrow{\Lambda}_{(i,j,k)}$ is

$$\iiint \overrightarrow{\Lambda}^*_{(i,j,k)} \cdot (L\chi) dV$$
$$= \int_{\theta=0}^{\pi} \int_{\phi=0}^{2\pi} \int_{R_{\text{in}}+\sum_n^m \xi_n^m Y_n^m(\theta,\phi)}^{R_{\text{out}}+\sum_n^m \Xi_n^m Y_n^m(\theta,\phi)} \overrightarrow{\Lambda}^*_{(i,j,k)}$$
$$\cdot (L\chi) r^2 \sin\theta dr d\phi d\theta, \tag{32}$$

where the asterisk symbol (*) in superscript is the complex conjugate operator. For governing Equations (3) and (6), $\overrightarrow{\Lambda}_{(i,j,k)}$ can be $\eta_i(r) \overrightarrow{R_j^k}(\theta, \phi)$, $\eta_i(r) \overrightarrow{S_j^k}(\theta, \phi)$, and $\eta_i(r) \overrightarrow{T_j^k}(\theta, \phi)$, where $\overrightarrow{R_j^k}(\theta, \phi)$, $\overrightarrow{S_j^k}(\theta, \phi)$ and $\overrightarrow{T_j^k}(\theta, \phi)$ are radial, consoidal, and toroidal vector spherical harmonics of the displacement field $\boldsymbol{u}$ respectively (Dahlen & Tromp 1998).

The integral of a scalar equation $L\chi$ with a trial function $\sigma_{(i,j,k)}$ is

$$\iiint \sigma_{(i,j,k)} \cdot (L\chi) dV$$
$$= \int_{\theta=0}^{\pi} \int_{\phi=0}^{2\pi} \int_{R_{\text{in}}+\sum_n^m \xi_n^m Y_n^m(\theta,\phi)}^{R_{\text{out}}+\sum_n^m \Xi_n^m Y_n^m(\theta,\phi)} \sigma_{(i,j,k)}$$
$$\cdot (L\chi) r^2 \sin\theta dr d\phi d\theta. \tag{33}$$

For Poisson's equation, the trial function $\sigma_{(i,j,k)}$ is $\eta_i(r)Y_j^k(\theta, \phi)$.

5. Integration on Surfaces

Now we will discuss how to solve boundary conditions on an asymmetric boundary. Suppose a boundary surface is described by

$$r(\theta, \phi) = r_0 + \sum_{n,m} \kappa_n^m Y_n^m(\theta, \phi), \tag{34}$$

then the radius vector of a point at (r, θ, ϕ) in this surface is

$$\overrightarrow{r} = r(\theta, \phi)\hat{r}, \tag{35}$$

where r_0, θ and ϕ are the mean radius of the sphere with same volume at this boundary surface, co-latitude and longitude, respectively. and the normalized normal vector $\hat{n}$ of this surface at the location $\boldsymbol{r}$ is

$$\hat{n} = \frac{\frac{\partial \overrightarrow{r}}{\partial \theta} \times \frac{\partial \overrightarrow{r}}{\partial \phi}}{\left| \frac{\partial \overrightarrow{r}}{\partial \theta} \times \frac{\partial \overrightarrow{r}}{\partial \phi} \right|}. \tag{36}$$

The area of this boundary surface is

$$\oiint dS = \int_{\theta=0}^{\pi} \int_{\phi=0}^{2\pi} \left| \frac{\partial \overrightarrow{r}}{\partial \theta} \times \frac{\partial \overrightarrow{r}}{\partial \phi} \right| d\phi d\theta. \tag{37}$$

The surface integral of a boundary condition is

$$\begin{aligned}
&\oiint \hat{n} \cdot \square \, dS \\
&= \int_{\theta=0}^{\pi} \int_{\phi=0}^{2\pi} (\hat{n} \cdot \square) \left| \frac{\partial \overrightarrow{r}}{\partial \theta} \times \frac{\partial \overrightarrow{r}}{\partial \phi} \right| d\phi d\theta \\
&= \int_{\theta=0}^{\pi} \int_{\phi=0}^{2\pi} \left(\frac{\partial \overrightarrow{r}}{\partial \theta} \times \frac{\partial \overrightarrow{r}}{\partial \phi} \right) \cdot \square \, d\phi d\theta,
\end{aligned} \tag{38}$$

where $\square$ is a vector or a tensor expression of the boundary conditions. As

$$\begin{aligned}
\frac{\partial \overrightarrow{r}}{\partial \theta} \times \frac{\partial \overrightarrow{r}}{\partial \phi} &= r^2 \sin\theta \hat{r} - rr_\theta \sin\theta \hat{\theta} - rr_\phi \hat{\phi} \\
&= r^2 \sin\theta \left[\hat{r} - \frac{1}{r}\left(r_\theta \hat{\theta} + \frac{r_\phi}{\sin\theta}\hat{\phi} \right) \right] \\
&= [r(\theta, \phi)]^2 \sin\theta [\hat{r} - \nabla r(\theta, \phi)],
\end{aligned} \tag{39}$$

warning that the last step in above equation, i.e., the expression by ∇r, is valid only at the boundary and in the related surface integrals in this section, then Equation (38) becomes

$$\begin{aligned}
&\oiint \hat{n} \cdot \square \, dS \\
&= \int_{\theta=0}^{\pi} \int_{\phi=0}^{2\pi} \{[\hat{r} - \nabla r(\theta, \phi)] \cdot \square\} [r(\theta, \phi)]^2 \sin\theta d\phi d\theta.
\end{aligned} \tag{40}$$

If the box symbol $\square$ is a vector continuation boundary condition: $\square = \Delta\boldsymbol{u} = \boldsymbol{u}^+ - \boldsymbol{u}^-$. Then multiply a trial function $\sigma_{(i,j,k)}$:

$$\begin{aligned}
0 &= \oiint \sigma_{(i,j,k)} \hat{n} \cdot \Delta\boldsymbol{u} dS \\
&= \int_{\theta=0}^{\pi} \int_{\phi=0}^{2\pi} \sigma_{(i,j,k)} \{[\hat{r} - \nabla r(\theta, \phi)] \cdot \Delta\boldsymbol{u}\} \\
&\quad \times [r(\theta, \phi)]^2 \sin\theta d\phi d\theta,
\end{aligned} \tag{41}$$

where $\sigma_{(i,j,k)} = Y_j^k(\theta, \phi)\eta_i(r)$.

Now suppose $\square$ is a tensor continuation boundary condition: $\square = \delta\overleftrightarrow{T} = \overleftrightarrow{T}^+ - \overleftrightarrow{T}^-$, then Equation (40) turns into

$$\begin{aligned}
0 &= \oiint \overrightarrow{\Lambda}_{(i,j,k)} \cdot [\hat{n} \cdot \delta\overleftrightarrow{T}] dS \\
&= \int_{\theta=0}^{\pi} \int_{\phi=0}^{2\pi} \overrightarrow{\Lambda}_{(i,j,k)} \cdot \{[\hat{r} - \nabla r(\theta, \phi)] \cdot \delta\overleftrightarrow{T}\} \\
&\quad \times [r(\theta, \phi)]^2 \sin\theta d\phi d\theta.
\end{aligned} \tag{42}$$

For a scalar continuation condition:

$$\delta a = a^+ - a^- = 0, \tag{43}$$

it is slightly tricky, for it is impossible to get a linear form of its surface integral in explicit formula, as there is a $\left| \frac{\partial \overrightarrow{r}}{\partial \theta} \times \frac{\partial \overrightarrow{r}}{\partial \phi} \right|$ in the denominator in Equation (36). So multiply Equation (43) by $\left| \frac{\partial \overrightarrow{r}}{\partial \theta} \times \frac{\partial \overrightarrow{r}}{\partial \phi} \right| \sin\theta$:

$$\left| \frac{\partial \overrightarrow{r}}{\partial \theta} \times \frac{\partial \overrightarrow{r}}{\partial \phi} \right| \sin\theta * \delta a = 0, \tag{44}$$

then the boundary condition (43) turns into

$$\begin{aligned}
0 &= \oiint \sigma_{(i,j,k)} \left| \frac{\partial \overrightarrow{r}}{\partial \theta} \times \frac{\partial \overrightarrow{r}}{\partial \phi} \right| \sin\theta * \delta a * \left(\frac{\partial \overrightarrow{r}}{\partial \theta} \times \frac{\partial \overrightarrow{r}}{\partial \phi} \right) d\phi d\theta \\
&= \int_{\theta=0}^{\pi} \int_{\phi=0}^{2\pi} \sigma_{(i,j,k)} \left| \frac{\partial \overrightarrow{r}}{\partial \theta} \times \frac{\partial \overrightarrow{r}}{\partial \phi} \right|^2 * \delta a * \sin\theta d\phi d\theta,
\end{aligned} \tag{45}$$

where

$$\begin{aligned}
&\left| \frac{\partial \overrightarrow{r}}{\partial \theta} \times \frac{\partial \overrightarrow{r}}{\partial \phi} \right|^2 \\
&= r^4 \sin^2\theta + r^2 [r_\theta \sin\theta]^2 + r^2 r_\phi^2 \\
&= r^4(1 - \cos^2\theta) + r^2 [r_\theta \sin\theta]^2 + r^2 r_\phi^2.
\end{aligned} \tag{46}$$

6. Earth Model

PREM is adopted here excluding the ocean. We divide this model into 12 layers according to PREM to describe the parameters such as density and Lamé parameters; and three layers to describe the variables such as the displacement vector field and the incremental potential scalar. The three layers are the inner core, the outer core and the mantle (with crust). Then the Earth model is modified by one order ellipticity by rotation. We solve the hydrostatic equilibrium figure by a more prototypic equation instead of Clairaut's equation in differential
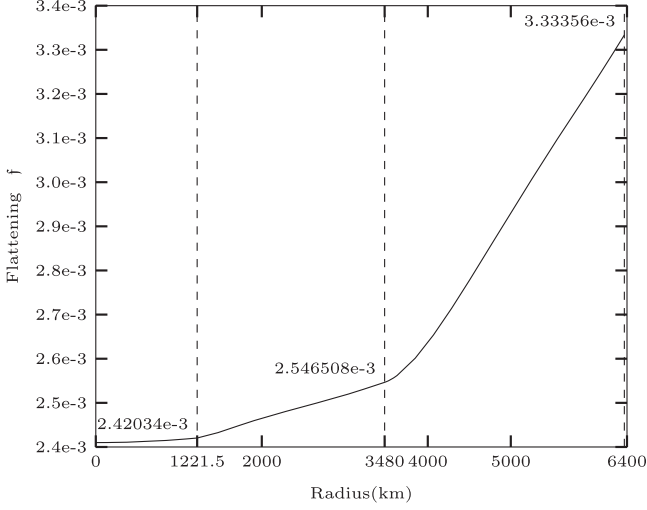
Figure 1. Profile of the flattening f.

form, which is (Moritz 1990; Huang et al. 2019)

$$\left(\frac{1}{r_0^n}\frac{d\epsilon_n^m}{dr_0} + \frac{n}{r_0^{n+1}}\epsilon_n^m\right)\int_0^{r_0}\rho q^2 dq$$

$$- \int_{r_0}^R \rho\frac{d}{dq}\left(\frac{\epsilon_n^m}{q^{n-2}}\right)dq + \frac{5\Omega^2}{12\pi G}\Big|_{\text{if } n=2, m=0} = 0. \quad (47)$$

This integro-differential equation is to be solved to get the ellipticity profiles $\epsilon_n^m(r_0)$ interior the Earth by our spectral element method. For a first-order approximated ellipsoid, an equipotential surface in the equilibrium figure is

$$r_S = r_0[1 + \epsilon_2^0 P_2(\cos\theta)], \quad (48)$$

where r_0 is the mean radius of the sphere with same volume surrounded by this boundary surface. The flattening f is

$$\mathfrak{f} = \frac{a - b}{a}, \quad (49)$$

where a, b are the equatorial radius and the polar radius respectively, and it can be proven that in first-order approximation (Moritz 1990)

$$\epsilon_2^0 = -\frac{2}{3}\mathfrak{f}. \quad (50)$$

Figure 1 shows the calculated profile of the flattening with respect to r. The flattening at the Earth's surface is $\mathfrak{f} = 1/299.98$ and that at CMB is $\mathfrak{f} = 1/392.70$.

After deformation, the density ρ, the Lamé parameters λ and μ, and the gravitational potential ψ are decomposed into spherical parts and non-spherical parts:

$$\rho(r_S) = \rho_0(r_S) + \delta\rho(r_S) \quad (51)$$

$$\lambda(r_S) = \lambda_0(r_S) + \delta\lambda(r_S) \quad (52)$$

$$\mu(r_S) = \mu_0(r_S) + \delta\mu(r_S) \quad (53)$$

$$\psi(r_S) = \psi_0(r_S) + \delta\psi(r_S), \quad (54)$$

where $\rho_0(r_S)$, $\lambda_0(r_S)$, $\mu_0(r_S)$, and $\psi_0(r_S)$ are the parameters before deformation. Dahlen (1968) gave the non-spherical parts as

$$\delta\rho(r_S) = \epsilon_2^0 r_S\frac{\partial\rho_0(r_S)}{\partial r_S}P_2(\cos\theta) \quad (55)$$

$$\delta\lambda(r_S) = \epsilon_2^0 r_S\frac{\partial\lambda_0(r_S)}{\partial r_S}P_2(\cos\theta) \quad (56)$$

$$\delta\mu(r_S) = \epsilon_2^0 r_S\frac{\partial\mu_0(r_S)}{\partial r_S}P_2(\cos\theta) \quad (57)$$

$$\delta\psi(r_S) = \epsilon_2^0 r_S\frac{\partial\psi_0(r_S)}{\partial r_S}P_2(\cos\theta). \quad (58)$$

Then the gravity $\boldsymbol{g}$ in the new equilibrium configuration is

$$\boldsymbol{g} = \nabla\{\psi + \frac{1}{3}\Omega^2 r_S^2[1 - P_2(\cos\theta)]\}. \quad (59)$$

7. Boundary Conditions at the Geocenter

For this FCN computation, the displacement field $\boldsymbol{u}$ is truncated as $\overrightarrow{T}_1^1 + (\overrightarrow{R}_2^1 + \overrightarrow{S}_2^1) + \overrightarrow{T}_3^1$ in its coupling chain of spheroidal and toroidal expansion. Vector spherical harmonics are expanded in power series in each subdomain, for instance, the terms with $\overrightarrow{S}_2^1$ are expanded as

$$\sum_{i=0}^{r_{max}} a_i r^i \overrightarrow{S}_2^1, \quad (60)$$

where r_{max} is the max power order, and a_i are unknown coefficients. $\overrightarrow{S}_2^1$ has the same expansion forms in the inner core, the fluid core, and the mantle, but the coefficients are different, for instance, a_i can be written as $a_i^{(IC)}$, $a_i^{(OC)}$ and $a_i^{(MT)}$ respectively. Similarly, we can obtain the expansions of $\overrightarrow{T}_1^1$, $\overrightarrow{R}_2^1$, $\overrightarrow{T}_3^1$ and V_1.

The boundary condition at the geocenter is required to be regular. This is a vague statement. For the free-oscillation equations, Crossley (1975) expanded the variables as power series,

$$y_i(r) = r^\alpha\sum_{\nu=0}^\infty A_{i,\nu}r^\nu,$$
$$i = 1, 2, \cdots, 8, \quad (61)$$

where $\{y_1, y_2, \cdots, y_8\}$ represented the three vector spherical harmonics components of the displacement field $\boldsymbol{u}$, the three components of $\hat{n}\cdot\overleftrightarrow{S}$, and the other two spherical harmonics coefficients of the incremental gravitational potential V_1 and a combination with its gradient. Then the power series were substituted into the PDEs, and one independent initial solution was obtained by picking α and a set of $A_{i,\nu}$ making PDEs finite

at the geocenter. Then three independent solutions combined into one general solution.

The approach in this work which is to establish several algebraic equations of the coefficients is different from that taken by Zhang & Huang (2019), For instance, Equation (3) has four set of algebraic equations for the vector spherical harmonics: $\overrightarrow{T}_1^1$, $\overrightarrow{R}_2^1$, $\overrightarrow{S}_2^1$, and $\overrightarrow{T}_3^1$. There are two algebraic equations in each set, for example, there are two equations corresponding with $\frac{1}{r}\overrightarrow{S}_2^1$ and $\frac{1}{r^2}\overrightarrow{S}_2^1$ respectively in $\overrightarrow{S}_2^1$ set. The equation for $\frac{1}{r}\overrightarrow{S}_2^1$ takes the form:

$$z_{i_1} + z_{i_2} + \cdots + z_{i_N} = 0. \tag{62}$$

This equation comes from putting the expansions of the displacement field $\boldsymbol{u}$

$$\boldsymbol{u} \approx \sum_{i=0}^{r_{\max}} a_i r^i \ \overrightarrow{T}_1^1 + \sum_{i=0}^{r_{\max}} b_i r^i \ \overrightarrow{R}_2^1$$
$$+ \sum_{i=0}^{r_{\max}} c_i r^i \ \overrightarrow{S}_2^1 + \sum_{i=0}^{r_{\max}} d_i r^i \ \overrightarrow{T}_3^1 \tag{63}$$

and the expansion of the incremental gravitational potential V_1

$$V_1 = \sum_{i=0}^{r_{\max}} e_i r^i \ Y_2^1 \tag{64}$$

into Equation (3) and filtering the terms with $\frac{1}{r}\overrightarrow{S}_2^1$. We use this approach in this paper.

8. Matrix

It is very complex and difficult to expand massive mathematical expressions and to integrate them in an asymmetric Earth model. So we write a computer algebra system in Common Lisp to implement these functions. After tedious symbol computations, we can get a large matrix. Each row corresponds a trial function, and each column corresponds an unknown coefficient. Finally there is still an unknown quantity ω in the matrix. ω is one of eigenfrequencies to be searched so that the determinant of the matrix must be zero. It is difficult to compute the determinant of a large matrix, so we use Singular Value Decomposition (SVD) algorithm to obtain an equivalent determinant. We use the reliable SVD routine of Linear Algebra PACKage (LAPACK).

For instance, suppose $r_{\max} = 5$, we will obtain three 124×124 matrices $\mathbb{M}_0$, $\mathbb{M}_1$ and $\mathbb{M}_2$, then the final matrix $\mathbb{M}$ is

$$\mathbb{M} = \mathbb{M}_0 + \omega\mathbb{M}_1 + \omega^2\mathbb{M}_2, \tag{65}$$

and $\mathbb{M}$ satisfies

$$\mathbb{M} \cdot \begin{cases} \overrightarrow{T}_1^1, \overrightarrow{R}_2^1, \overrightarrow{S}_2^1, \overrightarrow{T}_3^1, Y_2^1 \ \text{ terms in IC} \\ \overrightarrow{T}_1^1, \overrightarrow{R}_2^1, \overrightarrow{S}_2^1, \overrightarrow{T}_3^1, Y_2^1 \ \text{ terms in OC} \\ \overrightarrow{T}_1^1, \overrightarrow{R}_2^1, \overrightarrow{S}_2^1, \overrightarrow{T}_3^1, Y_2^1 \ \text{ terms in MT} \end{cases} = 0. \tag{66}$$
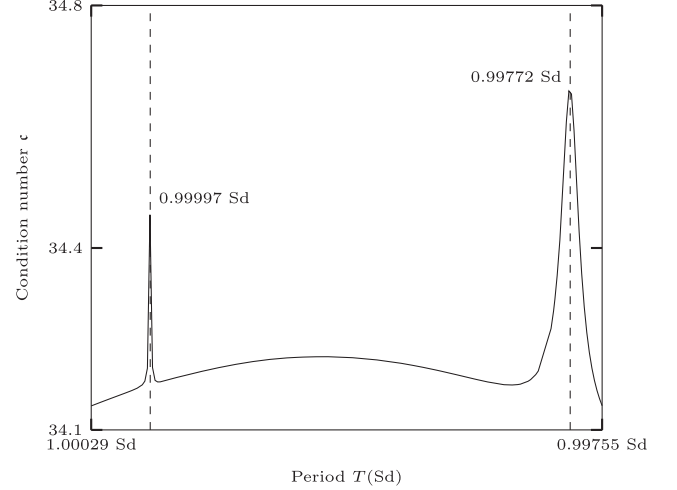

Figure 2. Condition number $\mathfrak{c}$ respect to period T, where $r_{\max} = 5$.

To find a normal mode of the Earth is equivalent to search an ω that satisfies the following equation:

$$\mathbb{M}_0 + \omega\mathbb{M}_1 + \omega^2\mathbb{M}_2 = 0. \tag{67}$$

If ω_* is a solution of Equation (67), then the determinant of its coefficient matrix:

$$\mathbb{M} = \mathbb{M}_0 + \omega_*\mathbb{M}_1 + \omega_*^2\mathbb{M}_2 \tag{68}$$

must be zero. However, it is virtually impossible to compute the determinant of a 124×124 matrix. An alternative way is to compute its condition number, and search for its maxima. The matrix $\mathbb{M}$ is decomposed by SVD into

$$\mathbb{M} = \mathbb{U}\mathbb{S}\mathbb{V}^*, \tag{69}$$

where $\mathbb{U}$ and $\mathbb{V}$ are unitary, and $\mathbb{S}$ is a diagonal matrix with non-negative real numbers on the diagonal. Suppose $\mathfrak{s}_{\max}$ is the largest diagonal entry and $\mathfrak{s}_{\min}$ is the smallest, then define the condition number $\mathfrak{c}$ as

$$\mathfrak{c} := \log \mathfrak{s}_{\max} - \log \mathfrak{s}_{\min}. \tag{70}$$

To search for the normal modes or eigen-periods (ω) of the dynamical system is transferred to search the zero-points of the determinant of the $\mathbb{M}$, also equivalent to search the maxima of $\mathfrak{c}$.

Figure 2 shows this condition number $\mathfrak{c}$ with respect to angular frequency ω ranging from $7.29e - 5$ to $7.31e - 5$ where $r_{\max} = 5$. There are two peaks in this range, which means there are two possible zero determinants, in other words, two possible normal modes.

9. Results

Tilt-over Mode (TOM) has the same period with the rigid Earth, which in theory should be exact 1 Sd. We can use TOM to evaluate the accuracy of our numerical solutions. Table 1

Table 1
Periods of TOM with Truncation of $\overrightarrow{T}_1^1 + (\overrightarrow{R}_2^1 + \overrightarrow{S}_2^1) + \overrightarrow{T}_3^1$

r_{max}	Angular Frequency (rad s^{-1})	Period (Sd)	Deviation
3	7.29232e-5	0.99997	−0.003%
4	7.29231e-5	0.99997	−0.003%
5	7.29231e-5	0.99997	−0.003%
6	7.29232e-5	0.99997	−0.003%
7	7.29240e-5	0.99996	−0.004%

Table 2
Periods of FCN with Truncation of $\overrightarrow{T}_1^1 + (\overrightarrow{R}_2^1 + \overrightarrow{S}_2^1) + \overrightarrow{T}_3^1$

r_{max}	Angular Frequency (rad s^{-1})	Period (Sd)
3	7.3098e-5	−412
4	7.3088e-5	−437
5	7.3088e-5	−437
6	7.3088e-5	−437
7	7.3088e-5	−437

Table 3
Periods of FCN with Truncation
of $\overrightarrow{T}_1^1 + (\overrightarrow{R}_2^1 + \overrightarrow{S}_2^1) + \overrightarrow{T}_3^1 + (\overrightarrow{R}_4^1 + \overrightarrow{S}_4^1) + \overrightarrow{T}_5^1$

r_{max}	Angular Frequency (rad s^{-1})	Period (Sd)
4	7.3088e-5	−437
5	7.3089e-5	−434
6	7.3089e-5	−434

shows the period of TOM with respect to the truncation order r_{max}. All the terms in the equations and the boundary conditions are accurate to the second order of ellipticity $(\epsilon_2^0)^2$ in our computation. When $3 \leqslant r_{max} \leqslant 7$, the absolute value of the deviation between our calculated and the theoretical value (i.e., 1.0 Sd) is less than 0.004% which means the accuracy and precision of our calculation is at the level of $(\epsilon_2^0)^2$. When $r_{max} \geqslant 8$, we cannot find an extremum of the equivalent determinant, because the power series has a disadvantage which is not normalized.

As the accuracy of calculated TOM is about −0.003%, we keep five digits explicitly in FCN results. Table 2 shows the results of FCN. When $r_{max} = 3$, the result does not seem to be good, because the basis functions are not enough. Increasing r_{max} from 4 to 7, the angular frequency of FCN converges to $7.3088e - 5$ and the corresponding period in the celestial reference frame is −437 Sd.

If the displacement field $\boldsymbol{u}$ is truncated as $\overrightarrow{T}_1^1 + (\overrightarrow{R}_2^1 + \overrightarrow{S}_2^1) + \overrightarrow{T}_3^1 + (\overrightarrow{R}_4^1 + \overrightarrow{S}_4^1) + \overrightarrow{T}_5^1$, we will obtain the period of FCN: −437, −434, and −434 Sd for $r_{max} = 4$, $r_{max} = 5$, and $r_{max} = 6$ respectively. Table 3 shows these results. It shows that increasing the truncation order of the coupling chain among the spheroidal and toroidal components can improve the results significantly and that the results can be also converged very well when taking $r_{max} = 5$.

10. Discussion

There are some possible reasons for the good results. First, the Galerkin method avoids using the derivatives of density and Lamé parameters, which may be not accurate enough in PREM comparing with the values of density and elastic Lamé parameters themselves. Huang & Zhang (2014) reported their numerical test, by the second approach (i.e., direct Runge–Kutta integration of the linear dynamical equations in which the derivatives of density and elastic Lamé parameters through the whole Earth are used) mentioned in Section 1, and showed that the calculated FCN period can be changed significantly if given some changes only in the input of the derivatives of density near CMB. For Lamé parameters, their derivatives are in the term $\nabla \cdot \overrightarrow{S}$ in the governing Equation (3), the Galerkin method multiplies a vector trial function $\overrightarrow{X}$ on the both sides of

Equation (3). It is easy to prove that (Dahlen & Tromp 1998)

$$
\begin{aligned}
\int_V \overrightarrow{X} \cdot (\nabla \cdot \overleftrightarrow{S}) dV &= \int_V \nabla \cdot (\overrightarrow{X} \cdot \overleftrightarrow{S}) dV - \int_V \nabla \overrightarrow{X} : \overleftrightarrow{S} dV \\
&= \int_S \hat{n} \cdot (\overrightarrow{X} \cdot \overleftrightarrow{S}) dS - \int_V \nabla \overrightarrow{X} : \overleftrightarrow{S} dV \\
&= \int_S (\overrightarrow{X} \cdot \hat{n} \cdot \overleftrightarrow{S}) dS - \int_V \nabla \overrightarrow{X} : \overleftrightarrow{S} dV.
\end{aligned}
\tag{71}
$$

From above equivalence, the integral of $\nabla \cdot \overrightarrow{S}$ turns into the integral of $\overrightarrow{S}$, so the derivatives of Lamé parameters are eliminated. For density, its derivative appears in the term $4\pi G \nabla \cdot (\rho_0 \boldsymbol{u})$ in Poisson's Equation (10) and in the term ρ_1 in Equations (6) and (7); the Galerkin method multiplies a trial scalar function f on the both sides of Equation (10). It is easy to prove that

$$
\begin{aligned}
\int_V f^* 4\pi G \nabla \cdot (\rho_0 \boldsymbol{u}) dV &= \int_S f^* 4\pi G \rho_0 \hat{n} \cdot \boldsymbol{u} dS \\
&- \int_V 4\pi G \rho_0 \nabla f \cdot \boldsymbol{u} dV.
\end{aligned}
\tag{72}
$$

So the derivative of the density in the term $\nabla \cdot (\rho_0 \boldsymbol{u})$ is eliminated. The boundary conditions (12), (11) can substitute the surface integrals $\int_S (\overrightarrow{X} \cdot \hat{n} \cdot \overleftrightarrow{S}) dS$ and $\int_S f^* 4\pi G \rho_0 \hat{n} \cdot \boldsymbol{u} dS$, which become the natural boundary conditions. Seyed-Mahmoud (1994) used the natural boundary conditions to deal with the rotational modes in fluid core.

For PREM (Dziewonski & Anderson 1981), by inversion of seismology data and normal modes, the layered structure and the crude initial profiles of density and Lamé parameters were reconstructed. Then these parameters were modified by the data of normal modes. Dziewonski & Anderson (1981) applied the Rayleigh's principle and the perturbation theory on normal modes, and his approach was only like the Galerkin method which replaced trial functions with the original displacement

field $\boldsymbol{u}$, and modified boundary conditions into natural boundary conditions. Their approach can invert the parameters as a whole, but may remove some details and smooth the profile curves including the derivatives of density and elastic Lamé parameters. Our approach also focuses on whole characteristics, and can neglect some details of the derivatives, for instance, some small jumps in the density profile. On the other hand, some fine details may affect linear momentum approach. Rogister & Rochester (2004) used Clairaut coordinates, and had the similar advantage that the ODEs governing free oscillations of a rotating hydrostatic Earth model contained no derivatives of material properties.

The second reason could be that we do not adopt the ESD proposed by Smith (1974) and used in the second approach mentioned in Section 1. The ESD transforms a first-order approximated ellipsoid into a sphere. For a point $\boldsymbol{P}(r_p, \theta_0, \phi_0)$ in an equipotential ellipsoidal surface, the corresponding point in ESD is $\boldsymbol{r}(r_0, \theta_0, \phi_0)$, which satisfies

$$r_p = r_0 - \frac{2}{3}\epsilon(r_0)P_2(\cos\theta). \tag{73}$$

This is actually a coordinate transformation; thus coordinates change and so do vectors, tensors and metrics. Moreover, the governing equations should also change, and the original governing equations do not usually hold true in the new coordinates. Generally speaking, the governing equations in an original coordinates should be rewritten in Hamilton form $H(p, q)$, where p and q are generalized momenta and coordinates respectively. In the new coordinates, the new Hamilton form is $K(P, Q)$, where P and Q are generalized momenta and coordinates respectively. It is not strict to solve $H(p, q)$ with P, Q, and a rigorous way is to use $K(P, Q)$.

In conclusion, we use the spectral element method (also called as the stratified Galerkin method) for integration of the dynamic equations of the realistic Earth model, and use the Tau method to combine the (asymmetric) boundary conditions, and our resulted FCN period converges very well and its 434 Sd result is very close to the observed value. It may suggest that the Earth's state may be closer to one of hydrostatic equilibrium than previously envisioned. We anticipate that these works will inspire more researches in this area.

Acknowledgments

ORCID iDs

Mian Zhang ⓘ https://orcid.org/0000-0002-5269-3764

References

Boyd, J. P. 2001, Chebyshev and Fourier Spectral Methods (Mineola, NY: Dover Publications)
Buffett, B. A., Mathews, P. M., & Herring, T. A. 2002, JGRB, 107, ETG
Crossley, D. J. 1975, GeoJI, 41, 153
Crossley, D. J., & Rochester, M. G. 2014, GeoJI, 198, 1890
Cui, X.-M., Sun, H.-P., Xu, J.-Q., Zhou, J.-C., & Chen, X.-D. 2018, EP&S, 70, 199
Dahlen, F. A. 1968, GeoJI, 16, 329
Dahlen, F. A. 1972, GeoJI, 28, 357
Dahlen, F. A., & Tromp, J. 1998, Theoretical Global Seismology (Princeton, NJ: Princeton Univ. Press)
Dehant, V. 1990, GeoJI, 100, 477
Dehant, V., & Defraigne, P. 1997, JGRB, 102, 27659
Dziewonski, A. M., & Anderson, D. L. 1981, PEPI, 25, 297
Gwinn, C. R., Herring, T. A., & Shapiro, I. I. 1986, JGRB, 91, 4755
Hough, S. S. 1895, RSPTA, 186, 469
Huang, C.-L., Dehant, V., & Liao, X.-H. 2004, GeoJI, 157, 831
Huang, C.-L., Dehant, V., Liao, X.-H., Van Hoolst, T., & Rochester, M. G. 2011, JGRB, 116, B03403
Huang, C.-L., Jin, W.-J., & Liao, X.-H. 2001, GeoJI, 146, 126
Huang, C.-L., & Liao, X.-H. 2003, GeoJI, 155, 669
Huang, C.-L., Liu, Y., Liu, C.-J., & Zhang, M. 2019, JGeod, 93, 297
Huang, C.-L., & Zhang, M. 2014, AGUFM, 2014, G13A
Jiang, X.-H., & Smylie, D. E. 1996, PEPI, 94, 159
Johnson, I. M., & Smylie, D. E. 1977, GeoJI, 50, 35
Kamruzzaman, M. 2021, PhD thesis, Univ. Lethbridge (Canada)
Karniadakis, G., & Sherwin, S. 2013, Spectral/hp Element Methods for Computational Fluid Dynamics (Oxford: Oxford Univ. Press)
Kopal, Z. 1980, Ap&SS, 70, 407
Malkin, Z. 2017, JGeod, 91, 839
Mathews, P. M., Buffett, B. A., Herring, T. A., & Shapiro, I. I. 1991, JGRB, 96, 8219
Mathews, P. M., Herring, T. A., & Buffett, B. A. 2002, JGRB, 107, ETG
Moon, W. 1982, GeoJI, 69, 431
Moritz, H. 1990, Science, Mind and the Universe (Karlsruhe: Wichmann), 1
Phinney, R. A., & Burridge, R. 1973, GeoJI, 34, 451
Rochester, M. G., Graham, G. A. C., & Malik, S. K. 1989, Continuum Mechanics and its Applications (Washington, DC: Hemisphere), 797
Rochester, M. G., Crossley, D. J., & Zhang, Y.-L. 2014, GeoJI, 198, 1848
Rochester, M. G., Jensen, O., & Smylie, D. 1974, GeoJI, 38, 349
Rogister, Y. 2001, GeoJI, 144, 459
Rogister, Y., & Rochester, M. G. 2004, GeoJI, 159, 874
Seyed-Mahmoud, B. 1994, PhD thesis, Memorial Univ. Newfoundland
Seyed-Mahmoud, B., Heikoop, J., & Seyed-Mahmoud, R. 2007, GApFD, 101, 489
Seyed-Mahmoud, B., & Moradi, A. 2014, PEPI, 227, 61
Seyed-Mahmoud, B., Moradi, A., Kamruzzaman, M., & Naseri, H. 2015, GeoJI, 202, 1146
Seyed-Mahmoud, B., Rochester, M. G., & Rogers, C. M. 2017, GeoJI, 209, 1455
Seyed-Mahmoud, B., & Rogister, Y. 2021, GApFD, 115, 648
Smith, M. L. 1974, GeoJI, 37, 491
Smylie, D. E., Jiang, X.-H., Brennan, B. J., & Sato, K. 1992, GeoJI, 108, 465
Song, X. 2011, in Differential Rotation of the Earth's Inner Core, Encyclopedia of Solid Earth Geophysics, ed. H. K. Gupta (Berlin: Springer), 118
Song, X., & Richards, P. G. 1996, Natur, 382, 221
Wahr, J. M. 1981, GeoJI, 64, 705
Wu, W.-J. 1993, PEPI, 75, 289
Zhang, M., & Huang, C.-L. 2014, AGUFM, 2014, G12A
Zhang, M., & Huang, C.-L. 2019, G&G, 10, 146
Zhou, Y.-H., Zhu, Q., Salstein, D. A., et al. 2016, AdSpR, 57, 2136